

Depleted Kondo Lattices.

F.F. Assaad

*Institut für Theoretische Physik III,
Universität Stuttgart, Pfaffenwaldring 57, D-70550 Stuttgart, Germany.*

We consider a two dimensional Kondo lattice model with exchange J and hopping t in which three out of four impurity spins are removed in a regular way. At the particle-hole symmetric point the model may be studied with quantum Monte Carlo methods without sign problems. In this model, a metallic phase survives up to arbitrarily low temperatures before being disrupted by magnetic fluctuations which open a gap in the charge sector. As a function of temperature, we study the formation of the heavy-electron state with emphasis on the coherence scale. Comparison with mean-field approximations, in particular the large- N approach, shows that the mean-field Kondo temperature shows next to perfect agreement with the coherence scale when the model is solved exactly. From the technical point of view a simple method to reduce size effects by up to an order of magnitude in temperature is discussed. PACS numbers: 71.27.+a, 71.10.-w, 71.10.Fd

I. INTRODUCTION

Kondo insulators as well as heavy fermion materials [1,2] are believed to be described by Kondo lattice models with antiferromagnetic exchange J and hopping t . In this framework, the Kondo insulator - exemplified by $\text{Ce}_3\text{Bi}_4\text{Pt}_3$ - corresponds to a special band filling in which there is exactly one conduction electron per impurity spin. The origin of the charge and spin gaps is easy to understand in the limit of large J/t where each conduction electron is trapped by an impurity spin to form a Kondo singlet. Starting from this point there are two ways of generating metallic states which will describe the heavy electron state. On one hand, one can remove conduction electrons thus leaving uncompensated impurity spins. In the limit $J/t \rightarrow \infty$ the problem maps onto the $U \rightarrow \infty$ Hubbard model where the Kondo singlets are represented by empty sites and the bachelor - or unscreened - spins by electrons [3]. Thus, a metallic state is expected. On the other hand one can keep the number of conduction electrons constant and deplete the lattice of impurity spins. Starting from $\text{Ce}_3\text{Bi}_4\text{Pt}_3$ this amounts in replacing Ce by La [4]. Each missing impurity spin liberates a conduction electron. As easily seen in the strong coupling limit this conduction electron is localized since its motion involves the breaking of adjacent Kondo singlets. Hence a bound state with magnetic properties appears within the gap [5]. If the depletion is *large* enough the induced localized levels may overlap coherently to form a metallic state.

In the next section, we first consider within a mean-

field approximation [6] both above describe routes to obtain metallic states. The paramagnetic solution of this mean-field approximation is nothing but the large- N (N corresponds to the $\text{SU}(N)$ symmetry of the impurity spins) saddle point [7–9]. Here, we concentrate on a special choice of depletion scheme for the localized spins. Three out of four impurity spins are removed in a regular way thus ensuring that in the limit $J/t \rightarrow \infty$ the ground state is metallic. At the mean-field level both routes to obtain a metallic state (doping and above describe depletion scheme) lead to the same metallic ground state: a Fermi-liquid with arbitrarily large effective mass (or arbitrarily low coherence temperature) as the coupling J/t is reduced. The mean-field solution has several pitfalls. For instance, the imaginary part of the self-energy vanishes at all temperatures, the Kondo scale corresponds to a phase transition rather than to a crossover scale and charge fluctuations on impurity sites are allowed since constraints are imposed only on average.

For depleted Kondo lattices it is possible to carry out auxiliary field quantum Monte Carlo (QMC) simulations without encountering the infamous sign problem. This comes with the restriction of particle-hole symmetry for the conduction band. Nevertheless this gives us the opportunity to compare *exact* results with mean-field approximations. There are two challenges to circumvent before achieving good results. The first one is the implementation of the exchange interaction J along with the constraint of singly occupied impurity sites. This problem has been solved in [10] and extensively discussed in [11]. The second challenge lies in controlling finite size effects stemming from the conduction electrons. This is extremely important in the framework of Kondo physics since screening takes place on an energy scale set by the Kondo temperature T_K which is exponentially small in the weak coupling limit. If the level spacing of the conduction electrons exceeds this small energy scale, finite size effect will dominate the result. In section IIIB we present a simple method to reduce by up to an order magnitude in temperature the onset of size effects in thermodynamic quantities (specific heat, spin and charge susceptibilities) for a given lattice size.

Section IV summarizes our numerical results. Ground state, thermodynamic and transport properties are computed on lattice sizes up to 500 sites. We show that our simulations reproduce the typical form of the resistivity versus temperature curve observed in heavy fermion materials: an initial rise as a function of decreasing temperature originating from the onset of screening of the magnetic impurities then followed by a sharp down-

turn signaling the onset of coherence between individual screening clouds. Energy scales as a function of coupling strength are computed and compared to the mean-field results. It is shown that the mean-field Kondo temperature reproduces precisely the coherence scale observed in the QMC simulations. The last section is devoted to conclusions.

II. MODELS AND MEAN-FIELD APPROXIMATION

Our starting point is the two-dimensional Kondo lattice model (KLM):

$$H(\{\vec{R}\}) = -t \sum_{\langle \vec{i}, \vec{j} \rangle, \sigma} (c_{\vec{i}, \sigma}^\dagger c_{\vec{j}, \sigma} + \text{H.c.}) + \sum_{\vec{R}} \vec{S}_{\vec{R}}^c \cdot \vec{S}_{\vec{R}}^f \quad (1)$$

Here \vec{i} runs over the lattice sites of a two dimensional square lattice: $\vec{i} = n\vec{a}_x + m\vec{a}_y$, $n, m : 1 \cdots L$ with \vec{a}_x, \vec{a}_y the lattice vectors. The set of lattice points $\{\vec{R}\}$ denote the positions of impurity spins. $c_{\vec{i}, \sigma}^\dagger$ creates a conduction electron on site \vec{i} with z-component of spin σ and $\vec{S}_{\vec{R}}^f = \frac{1}{2} \sum_{\sigma, \sigma'} f_{\vec{R}, \sigma}^\dagger \vec{\sigma}_{\sigma, \sigma'} f_{\vec{R}, \sigma'}$ are the spin 1/2 operators with $\vec{\sigma}$ the Pauli spin matrices. A similar definition holds for $\vec{S}_{\vec{R}}^c$. Since the KLM stems from the strong coupling limit of the periodic Anderson model [12] the charge degrees of freedom on the f-sites are frozen. Hence, a constraint of one electron per f-site holds for KLM.

In the notation of Eq. 1 the usual KLM model is obtained when $\vec{R} = n\vec{a}_x + m\vec{a}_y$ (see Fig. 1a). In principle, the depletion scheme of impurity spins can be random - a situation which would reflect the experimental realization - or regular. As a first step we have chosen a regular depletion and considered $\vec{R} = n[2\vec{a}_x] + m[\vec{a}_x + 2\vec{a}_y]$ (see Fig. 1b). For now onwards we will refer to this model as the depleted Kondo lattice model (DKLM). The unit cell of the DKLM has five orbitals: one localized for the impurity spin and four delocalized for the conduction electrons. The Bravais lattice is spanned by the lattice vectors: $\vec{a}_1 = 2\vec{a}_x$ and $\vec{a}_2 = \vec{a}_x + 2\vec{a}_y$.

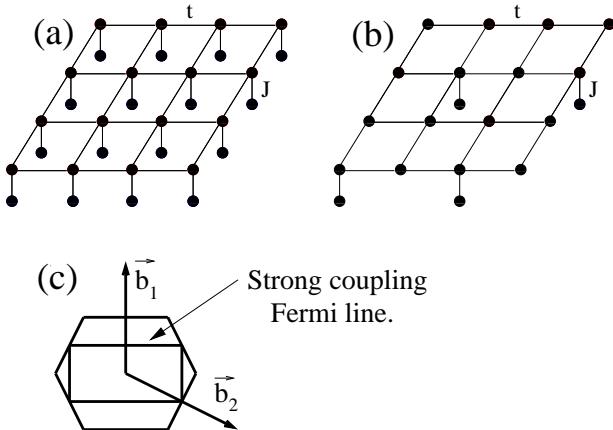


FIG. 1. (a) The standard KLM. The square lattice is spanned by the lattice vectors \vec{a}_x, \vec{a}_y . (b) The depleted KLM (DKLM). The corresponding Bravais lattice is spanned by $2\vec{a}_x$ and $\vec{a}_x + 2\vec{a}_y$. Each unit cell contains a single localized orbital for the impurity spin and four delocalized orbitals accommodating the conduction electrons. In both (a) and (b) the top layer denotes the conduction electrons with hopping matrix element t . The bottom layer are the magnetic impurities which couple to the conduction electrons via the exchange J . (c) the Brillouin zone of the DKLM. The reciprocal lattice vectors read $\vec{b}_1 = \frac{\pi}{a}(0, 1)$ and $\vec{b}_2 = \frac{\pi}{a}(1, -1/2)$

Having defined the model, we now address the question: to which degree does the KLM at $n_c < 1$ have the same physics as the DKLM at $n_c = 4$? Here n_c corresponds to the number of conduction electrons per unit cell. As mentioned previously, in the strong coupling limit the KLM with band filling n_c maps onto the $U \rightarrow \infty$ Hubbard model with band filling $\tilde{n}_c = 1 - n_c$ [3]. The nature of the metallic state is not clear due to the strong correlations. However for fillings far from the doping induced Mott metal-insulator transition, $\tilde{n}_c = 1$, it is reasonable to believe that beyond the one-dimensional case the ground state is a Fermi liquid as described for example by a Gutzwiller approximation. Due to the special choice of the depletion, the strong coupling DKLM at $n_c = 4$ is a Fermi liquid. In this limit, each impurity spin will capture a conduction electron and the remnant conduction electrons will form the metallic state. To be more precise at $J/t \rightarrow \infty$ we obtain a three band model, where a single conduction band crosses the Fermi level, $\epsilon_F = 0$. The thus obtained strong coupling Fermi line is shown in Fig. 1c.

In the weak coupling limit, we can address the above question within a mean-field approximation [6]. One can write the KLM and DKLM models as:

$$H(\{\vec{R}\}) = \sum_{\vec{k}, \sigma} \epsilon(\vec{k}) c_{\vec{k}, \sigma}^\dagger c_{\vec{k}, \sigma} \quad (2)$$

$$+ \frac{J}{4} \sum_{\vec{R}} (f_{\vec{R}, \uparrow}^\dagger f_{\vec{R}, \uparrow} - f_{\vec{R}, \downarrow}^\dagger f_{\vec{R}, \downarrow}) (c_{\vec{R}, \uparrow}^\dagger c_{\vec{R}, \uparrow} - c_{\vec{R}, \downarrow}^\dagger c_{\vec{R}, \downarrow})$$

$$- \frac{J}{4} \sum_{\vec{R}} (f_{\vec{R}, \downarrow}^\dagger c_{\vec{R}, \downarrow} + c_{\vec{R}, \uparrow}^\dagger f_{\vec{R}, \uparrow})^2 + (f_{\vec{R}, \uparrow}^\dagger c_{\vec{R}, \uparrow} + c_{\vec{R}, \downarrow}^\dagger f_{\vec{R}, \downarrow})^2$$

where the last term accounts precisely for the spin flip terms: $\frac{J}{2} \sum_{\vec{R}} (f_{\vec{R}, \uparrow}^\dagger f_{\vec{R}, \downarrow} c_{\vec{R}, \downarrow}^\dagger c_{\vec{R}, \uparrow} + f_{\vec{R}, \downarrow}^\dagger f_{\vec{R}, \uparrow} c_{\vec{R}, \uparrow}^\dagger c_{\vec{R}, \downarrow})$. With the above rewriting of the KLM we can introduce order parameters both for magnetism and Kondo screening.

$$\frac{1}{2} \langle f_{\vec{R}, \uparrow}^\dagger f_{\vec{R}, \uparrow} - f_{\vec{R}, \downarrow}^\dagger f_{\vec{R}, \downarrow} \rangle = m_f e^{i\vec{Q} \cdot \vec{R}}$$

$$\frac{1}{2} \langle c_{\vec{R}, \uparrow}^\dagger c_{\vec{R}, \uparrow} - c_{\vec{R}, \downarrow}^\dagger c_{\vec{R}, \downarrow} \rangle = -m_c e^{i\vec{Q} \cdot \vec{R}} \quad \text{and}$$

$$\langle f_{\vec{R}, \downarrow}^\dagger c_{\vec{R}, \downarrow} + c_{\vec{R}, \uparrow}^\dagger f_{\vec{R}, \uparrow} \rangle = \langle f_{\vec{R}, \uparrow}^\dagger c_{\vec{R}, \uparrow} + c_{\vec{R}, \downarrow}^\dagger f_{\vec{R}, \downarrow} \rangle = -V. \quad (3)$$

where \vec{Q} correspond to the relevant wave vector for mag-

netic order. Concentrating in a first step on paramagnetic solutions $m_s = m_f = 0$ we obtain the mean-field Hamiltonian

$$\begin{aligned}
H = & -t \sum_{\langle \vec{i}, \vec{j} \rangle, \sigma} \left(c_{\vec{i}, \sigma}^\dagger c_{\vec{j}, \sigma} + \text{H.c.} \right) - \mu \sum_{\vec{i}, \sigma} c_{\vec{i}, \sigma}^\dagger c_{\vec{i}, \sigma} \\
& + \frac{JV}{2} \sum_{\vec{R}, \sigma} \left(f_{\vec{R}, \sigma}^\dagger c_{\vec{R}, \sigma} + \text{H.c.} \right) \\
& + \lambda \sum_{\vec{R}} \left(\sum_{\sigma} f_{\vec{R}, \sigma}^\dagger f_{\vec{R}, \sigma} - 1 \right) + \frac{JN_{\text{imp}}V^2}{2} \quad (4)
\end{aligned}$$

where μ corresponds to the chemical potential, λ to a Lagrange multiplier enforcing the constraint of single occupancy on the f -sites on average and N_{imp} is the number of impurity spins. The saddle point equations, $\frac{\partial F}{\partial \lambda} = \frac{\partial F}{\partial V} = 0$, $\frac{1}{L^2} \frac{\partial F}{\partial \mu} = n_c$ where F is the free energy may then be solved to obtain the mean-field solution. The thus obtained saddle point corresponds precisely to that obtained in the large- N approximation [7–9].

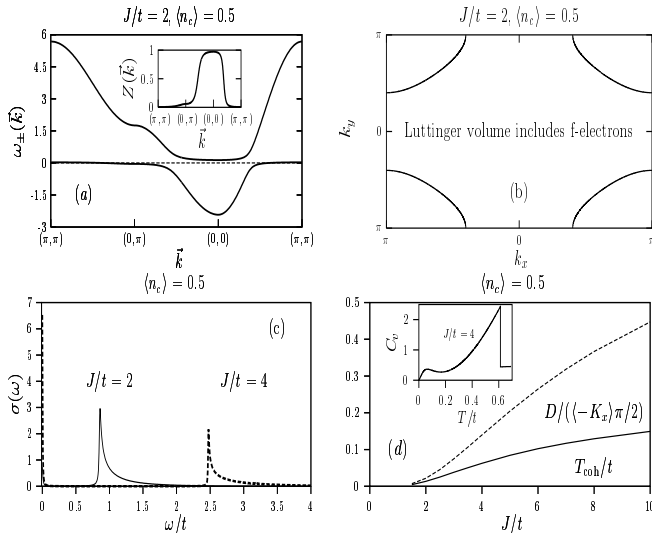


FIG. 2. Paramagnetic mean-field solution of the KLM at $n_c = 0.5$ (a) The band structure. Energies are measured with respect to the Fermi energy. The inset corresponds to the quasiparticle weight of the conduction band. (b) Fermi line. (c) Optical conductivity. Note that there is a Drude peak at $\omega = 0$. (d) Drude weight normalized by the sum rule as well as the coherence temperature as a function of J/t . The inset corresponds to the specific heat from which we obtain the coherence temperature. (see text)

Fig. 2 summarizes the paramagnetic mean-field solution for the KLM at $n_c = 0.5$. The band structure plotted in Fig. 2a consists of two bands (hybridized bands). As apparent, the band at the Fermi energy is flat and has a small quasiparticle weight (Fig. 2a inset). The corresponding Fermi surface (Fig. 2b), covers 75% of the Brillouin zone, so that both f -electrons and conduction electrons are included in the Luttinger volume. Given the band structure, the optical conductivity follows (Fig. 2c).

The large mass (i.e. combined small quasiparticle weight and flat dispersion relation) of the conduction electrons at the Fermi energy leads to a small Drude weight. The feature at higher frequencies are nothing but interband transitions. The Drude weight normalized by the sum rule as a function of J/t is plotted in Fig. 2d. At small values of J/t it becomes arbitrarily small reflecting the large mass of the charge carries. Along with the small Drude weight one expects a small coherence temperature. The coherence temperature (T_{coh}) - the energy scale at which the Fermi liquid character of the ground state becomes apparent - may be defined for example by the energy scale below which the specific heat is linear in T (inset Fig. 2d). As expected the J/t dependence of T_{coh} tracks the Drude weight. In the mean-field approach the Kondo temperature, T_K , corresponds to the temperature scale at which the order parameter V vanishes. Below T_K the magnetic impurities are screened. In the mean-field approximation, this screening does not take place via the formation of a many-body state of the impurity spin and conduction electrons but via charge fluctuations on the impurity sites. In this approximation, charge fluctuations are allowed since the constraint of single occupancy of f -sites is only imposed on average. As apparent by the jump in the specific heat (see inset of Fig. 2d) T_K corresponds to a phase transition rather than to a crossover scale. For a recent discussion of the Kondo and coherence scales within this approximation, the reader is referred to [9].

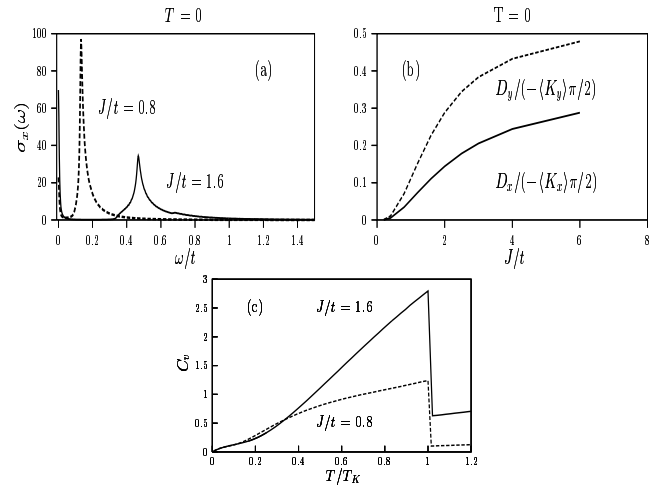


FIG. 3. Paramagnetic mean-field solution for the DKLM at $n_c = 4$. (i.e. the unit cell contains four conduction electrons) (a) Optical conductivity. (b) Drude weight normalized by the sum rule. (c) Specific heat versus T/T_K .

We now turn our attention to the DKLM. Figs. 3a,b plot the optical conductivity as well as the Drude weight versus J/t within the paramagnetic mean-field approximation. As apparent, there is a clear similarity with the above presented results for the KLM. From the specific heat data, (Fig. 3 c) one can extract the coherence tem-

perature. Here, some care has to be taken since the model has a van-Hove singularity at the Fermi level. Hence the coherence temperature corresponds to the energy scale below which the specific heat follows a $T \ln(1/T)$ law. Hence $T_{\text{coh}} \sim 0.1T_K$ for the considered couplings.

Next, we consider magnetic degrees of freedom for the DKLM. As mentioned above, at $J/t = \infty$ the model maps onto free electrons. The underlying particle-hole symmetry of the model directly leads to nesting so that the $J/t = \infty$ point will be unstable to magnetic ordering with wave vector $\vec{b}_1/2$ (Fig. 1c). At weak couplings the Ruderman-Kittel-Kasuya-Yosida (RKKY) interaction favors magnetic order rather than Kondo screening [13]. Hence, for all values of J/t we anticipate a magnetically ordered ground state. Fig. 4 plots the mean-field transition temperatures corresponding to Kondo screening, T_K , (below T_K , $V \neq 0$) and magnetism, T_S ($m_s \neq 0$, $m_f \neq 0$). As apparent, magnetic order is always present. For values of $J/t > 0.8$ the mean-field Kondo scale exceeds the magnetic scale T_S . For this parameter range and as a function of decreasing temperature, one expects to be able to study the formation of the heavy electron state prior to the onset of magnetic fluctuations which due to nesting will drive the system to an insulator. The QMC simulations presented in section IV are aimed at studying this crossover.

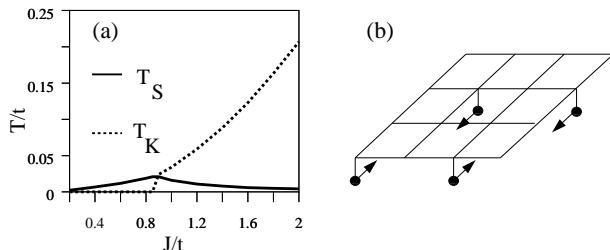


FIG. 4. (a) Mean-field energy scales for the DKLM at $n_c = 4$. T_K corresponds to the Kondo scale below which $V \neq 0$. T_S corresponds to a magnetic energy scale below which magnetic ordering with wave vector $\vec{Q} = \vec{b}_1/2$ – schematically shown in Fig. (b) – occurs. T_K and T_S mark phase transitions. For $J/t > 0.8$ both Kondo screening ($V \neq 0$) and magnetic ordering ($m_s \neq 0$, $m_f \neq 0$) are present in the ground state. At $J/t < 0.8$ the Kondo scale vanishes since in the mean-field approximation magnetic ordering freezes the impurity spins. The coherence temperature (not plotted in the figure) lies roughly an order of magnitude lower than the Kondo scale. Hence for most of the considered couplings it will be masked by the magnetic instability.

III. NUMERICAL TECHNIQUES

In this section we will first briefly summarize the numerical techniques used. We then turn our attention on a simple method to dramatically reduce the size effects for the simple case of free electrons. This is the key for producing size independent results down to low temperatures for the DKLM. However, this method is general

and may prove useful for other applications.

A. Quantum Monte Carlo algorithms

We have used ground state and finite temperature versions of the auxiliary field QMC method to investigate the DKLM. The $T = 0$ method is based on the equation:

$$\frac{\langle \Psi_0 | O | \Psi_0 \rangle}{\langle \Psi_0 | \Psi_0 \rangle} = \lim_{\Theta \rightarrow \infty} \frac{\langle \Psi_T | e^{-\Theta H_{DKLM}} O e^{-\Theta H_{DKLM}} | \Psi_T \rangle}{\langle \Psi_T | e^{-2\Theta H_{DKLM}} | \Psi_T \rangle} \quad (5)$$

where $|\Psi_T\rangle$ is required to be non-orthogonal to the ground state $|\Psi_0\rangle$. Finite temperature properties are calculated in the grand canonical ensemble via:

$$\langle O \rangle = \frac{\text{Tr} [e^{-\beta H_{DKLM}} O]}{\text{Tr} [e^{-\beta H_{DKLM}}]}. \quad (6)$$

Details of how to implement the QMC method without generating a sign problem in the particle-hole filled case have been introduced and extensively described for the KLM in Refs [10,11]. Since precisely the same *tricks* may be used for the DKLM, we refer the reader to those articles for further details. We now concentrate on another important issue, size effects, which become extremely severe when one wishes to study metallic states down to low temperatures.

B. Size effects and magnetic fields

Reducing size effects in numerical simulations is important, since many models of correlated electron systems may be solved numerically only on *small* lattices. Size effects become particularly severe when the ground state turns out to be a metallic state with large coherence temperature. On the other hand, insulators are characterized by the localization of the wave function and are hence rather insensitive to boundary conditions on finite sized systems. It thus becomes apparent, that the worst case scenario for severe size effects are just free electrons in a tight binding approximation:

$$H = -t \sum_{\langle i,j \rangle} c_i^\dagger c_j + \text{H.c.} \quad (7)$$

In many cases before turning on the interaction which will automatically restrict the size of the lattice under consideration it is important to control size effects for this simple case. We will concentrate on the two dimensional case on a torus geometry which for the above model reduces to imposing periodic boundary conditions: $c_{i+L\vec{e}_x}^\dagger = c_i^\dagger$, $c_{i+L\vec{e}_y}^\dagger = c_i^\dagger$ where L is the linear length of the lattice lying in the \vec{e}_x, \vec{e}_y plane.

To reduce size effects on thermodynamic quantities one may in principle consider the Hamiltonian:

$$H(L) = \sum_{\langle \vec{i}, \vec{j} \rangle} t_{\vec{i}, \vec{j}}(L) c_i^\dagger c_j + \text{H.c.} \quad (8)$$

where $t_{\vec{i}, \vec{j}}(L)$ are arbitrary hopping parameters which have to satisfy

$$\lim_{L \rightarrow \infty} t_{\vec{i}, \vec{j}}(L) = -t. \quad (9)$$

Clearly this choice of hopping matrix elements on finite lattices will break the lattice symmetry. This is a price we are willing to pay provided that the convergence as a function of system size of thermodynamics quantities is greatly improved. Eq. 9 nevertheless guarantees that in the thermodynamic limit this symmetry is restored. To determine the hopping matrix elements $t_{\vec{i}, \vec{j}}(L)$ so as to reduce size effects on say the specific heat, $C_v(L, T) = \frac{\partial E(L)}{\partial T}$, one may minimize

$$\chi^2 = \sum_T [C_v(L, T) - C_v(L = \infty, T)]^2 \quad (10)$$

where the sum extends over a given range of temperatures. Taking into account only amplitude modulations of the hopping matrix elements leads already to a cumbersome minimization problem which does not provide satisfactory results.

Instead of carrying out a complicated minimization problem we can try to guess which matrix elements $t_{\vec{i}, \vec{j}}(L)$ will minimize size effects. It turns out that introducing a magnetic field produces remarkable results. The magnetic field is introduced via the Peirls phase factors:

$$H(L) = -t \sum_{\langle \vec{i}, \vec{j} \rangle} e^{\frac{2\pi i}{\Phi_0} \int_{\vec{i}}^{\vec{j}} \vec{A}_L(\vec{l}) \cdot d\vec{l}} c_i^\dagger c_j + \text{H.c.} \quad (11)$$

with $\vec{B}_L(\vec{x}) = \vec{\nabla} \times \vec{A}_L(\vec{x})$ and Φ_0 the flux quanta. The torus geometry imposes restrictions on the \vec{B}_L field. Since, a translation in the argument of the vector potential may be absorbed in a gauge transformation:

$$\begin{aligned} \vec{A}_L(\vec{x} + L\vec{e}_x) &= \vec{A}_L(\vec{x}) + \vec{\nabla} \chi_x(\vec{x}), \\ \vec{A}_L(\vec{x} + L\vec{e}_y) &= \vec{A}_L(\vec{x}) + \vec{\nabla} \chi_y(\vec{x}), \end{aligned} \quad (12)$$

we chose, the boundary condition

$$c_{\vec{i}+L\vec{e}_x}^\dagger = e^{\frac{2\pi i}{\Phi_0} \chi_x(\vec{i})} c_i^\dagger, \quad c_{\vec{i}+L\vec{e}_y}^\dagger = e^{\frac{2\pi i}{\Phi_0} \chi_y(\vec{i})} c_i^\dagger \quad (13)$$

to satisfy the requirement:

$$[H(L), T_{L\vec{e}_x}] = [H(L), T_{L\vec{e}_y}] = 0. \quad (14)$$

Here, $T_{\vec{x}}$ corresponds to a translation by \vec{x} . However, magnetic translations operators belong to the magnetic algebra [14]:

$$T_{L\vec{e}_x} T_{L\vec{e}_y} = e^{-i2\pi \frac{(L\vec{e}_x \times L\vec{e}_y) \cdot \vec{B}}{\Phi_0}} T_{L\vec{e}_y} T_{L\vec{e}_x}. \quad (15)$$

Thus, to obtain a single valued wave function the condition of flux quantization has to be satisfied: $\frac{(L\vec{e}_x \times L\vec{e}_y) \cdot \vec{B}}{\Phi_0} = n$ where n is an integer. Here, we consider a static magnetic field running along the z -axis perpendicular to the x, y plane in which the lattice lies. Hence, the smallest magnetic field which we can consider on a given lattice size satisfies:

$$\frac{BL^2}{\Phi_0} = 1. \quad (16)$$

With this choice of magnetic field and associated vector potential Eq. 9 holds.

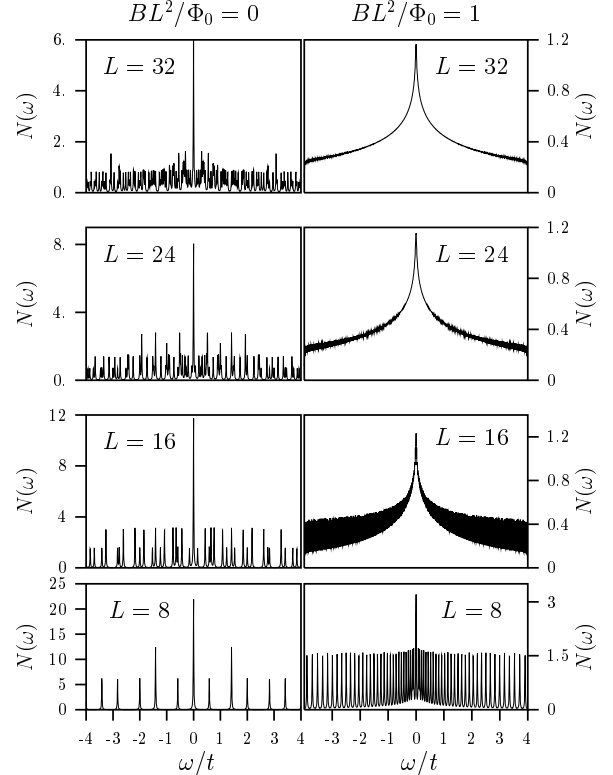


FIG. 5. Density of states $N(\omega) = \frac{1}{N} \sum_r N(r, \omega)$ with (right column) and without (left column) magnetic field. Here, we consider $\delta = 0.01t$.

To illustrate the reduction of size effects caused by the inclusion of the magnetic field, we first consider the single particle density of states. In a basis where $H(L)$ is diagonal, $H(L) = \sum_{n=1}^N \epsilon_n \gamma_n^\dagger \gamma_n$ with $c_n^\dagger = \sum_m \gamma_m^\dagger U_{m,n}^\dagger$ and $U^\dagger U = I$, the local density of states reads:

$$N(r, \omega) = \text{Im} \sum_n^N \frac{|U_{n,r}|^2}{\epsilon_n - \omega - i\delta} \quad (17)$$

where δ is a positive infinitesimal and N the total number of sites. Since the magnetic field breaks translation invariance (it is the site dependent vector potential which

enters the Hamiltonian) $N(r, \omega)$ is site dependent. Averaging over sites yields the density of states $N(\omega)$ plotted in Fig. 5. As apparent, without the magnetic field and up to $L = 32$, $N(\omega)$ is dominated by size effects for the considered value of $\delta = 0.01t$. In contrast, the presence of the magnetic field provides remarkable improvements. In particular the van-Hove singularity is well reproduced already on $L = 16$ lattices and at $L = 32$ the result is next to exact for the considered value of δ . It is instructive to look at the $L = 8$ case with and without magnetic fields. When B is turned on, the degeneracy of levels is lifted. Each level - apart from the $\epsilon_n = 0$ level which is two fold degenerate - is nondegenerate. This is precisely what one expects for Landau levels which have degeneracy $L^2 B / \Phi_0$ which is unity in our case. This provides an intuitive understanding of why the method works so well. Since each level becomes singly degenerate, the single particle states cover homogeneously the the energy range of the bandwidth. Clearly this can only be achieved by breaking the lattice symmetry on finite sized systems.

We now turn our attention to the specific heat coefficient $\gamma = C_v/T$ (see Fig. 6). As apparent, for a given system size, the inclusion of the magnetic field provides a gain of more than one order of magnitude in the temperature scale at which size effects set in. In particular the $\ln(1/T)$ behavior of γ due to the van-Hove singularity becomes apparent already on $L = 6$ lattices.

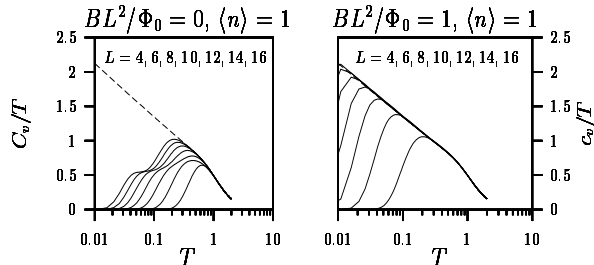


FIG. 6. Specific versus temperature with (right panel) and without (left panel) magnetic field. The curves from right to left correspond to increasingly large lattices as denoted in the figure. The dashed line corresponds to the exact result.

Upon inspection a similar improvement is obtained for the spin susceptibility (see Fig. 7). Note that since we are dealing with free electrons the charge and spin susceptibilities are identical.

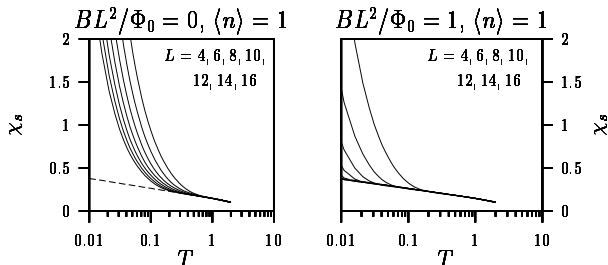


FIG. 7. Same as Fig. 6 but for the spin susceptibility.

One crucial question is whether the magnetic field will introduce a sign problem in the numerical simulations. It turns out that for DKLM at the particle-hole symmetric point it does not [11]. Hence we can incorporate it in our simulations and benefit from the above demonstrated drastic improvement in reduction of size effects.

Other schemes have been proposed to reduce size effects. In particular, averaging over boundary conditions has been suggested [15,16]. This method has the advantage of not breaking translation symmetry. However, the averaging requires several simulations and is hence computationally expensive. In contrast with the presented method the improvement in reduction of size effects is obtained within a single simulation.

IV. NUMERICAL RESULTS

Our numerical results for the DKLM are summarized in this section. We first concentrate on ground-state properties and check for magnetic ordering as a function of J/t . Various thermodynamic quantities (specific heat, spin and charge susceptibilities) as well as the optical conductivity and hence resistivity are then analyzed as a function of temperature at different values of J/t .

A. Spin-spin correlations at $T = 0$

To detect long-range magnetic ordering, we compute the spin-spin correlation function at $T = 0$:

$$S(\vec{Q}) = \sum_{\vec{R}} e^{i\vec{R} \cdot \vec{Q}} \frac{4}{3} \langle \vec{S}_{\vec{R}=0}^f \cdot \vec{S}_{\vec{R}}^f \rangle. \quad (18)$$

Here we consider $\vec{Q} = \vec{b}_1/2$ and the sum runs over the impurity spins. In the presence of long-range magnetic order, $S(\vec{Q})$ is an extensive quantity so that the staggered moment, $m_s = \lim_{L \rightarrow \infty} \sqrt{S(\vec{Q})/L^2}$, is finite. L^2 denotes the number of unit-cells.

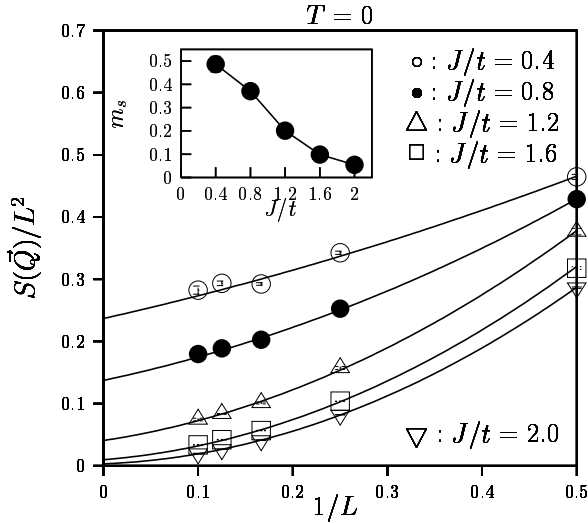


FIG. 8. $S(\vec{Q})$ at $T = 0$ for the DKLM as a function of system size and various values of J/t . The $L = 10$ point corresponds to a lattice of 10×10 unit cells and hence 500 orbitals. After extrapolation to the thermodynamic limit, we obtain the staggered moment plotted in the inset.

Figure 8 plots $S(\vec{Q})$ for various values of J/t . The inset in Fig. 8 plots the staggered moment obtained after extrapolation of $S(\vec{Q})$ to the thermodynamic limit. The data is thus consistent with long-range magnetic ordering at least up to $J/t = 2$. Clearly as J/t grows and the staggered moment becomes small, it is increasingly hard to distinguish it from zero. Nevertheless, and based on the mean-field result, we expect the staggered moment to vanish only in the limit $J/t \rightarrow \infty$.

Following arguments put forward in Ref. [11] Kondo screening and magnetic ordering to coexist: impurities are partially screened and the remnant magnetic moment orders. Depending upon the relative energy gains of both mechanisms a staggered moment of arbitrary magnitude can be produced. In the weak coupling limit, the energy gain for magnetism is the RKKY interaction. This interaction leads to an effective Heisenberg model between impurity spins with exchange $J_{RKKY}(\vec{q}) = -J^2 \text{Re}\chi(\vec{q}, \omega = 0)$ where $\chi(\vec{q}, \omega)$ corresponds to the spin susceptibility of the conduction electrons. On the other hand screening occurs on an energy scale set by the Kondo temperature: $T_K \sim W e^{-W/J}$ where W is the band width. Hence for small values of J/t the system will gain energy by ordering magnetically. Although the wave vector of magnetic ordering will depend on the details of the spin susceptibility, this source of energy gain is present irrespective of the band structure. On the other hand, the strong coupling result is an artifact of the model. In this limit, if Kondo screening were complete, a nested Fermi surface would be produced as in the $J/t \rightarrow \infty$ limit. Hence, in the ground state, the system will always gain energy by keeping Kondo screening partial. The remnant magnetic moment will order with the nesting wave vector thereby opening a gap and gaining

energy.

Were it not for nesting a finite critical value of the coupling J/t at which a quantum phase transition between ordered and disordered magnetic states would occur. Unfortunately, this is beyond the scope of the QMC since the absence of particle-hole symmetry and hence nesting leads to a sign problem.

B. Transport and thermodynamic properties.

Here, we consider finite temperature properties of the model. As discussed above, the ground state is a magnetic insulator irrespective of J/t . The salient features of the model however, lie in its thermodynamic properties.

We first consider the real part of the optical conductivity as obtained from the Kubo formula, $\sigma(\omega, T)$. This quantity is related to the imaginary time current-current correlation functions via:

$$\langle J(\tau)J(0) \rangle = \int d\omega K(\omega, \tau) \sigma(\omega, T)$$

$$\text{with } K(\omega, \tau) = \frac{1}{\pi} \frac{e^{-\tau\omega} \omega}{1 - e^{-\beta\omega}}. \quad (19)$$

Here J is the current operator along the x or y lattice direction and $\langle \rangle$ represents an average over the finite-temperature ensemble. The above inverse Laplace transform, to obtain the optical conductivity is carried out with the ME [17] method. We use the paramagnetic mean-field solution with substantial broadening as default model. Note that the order parameter V^2 which is proportional to the spin-spin correlation between the conduction electron and impurity spin is estimated from the Monte Carlo run and not by solving the saddle point equations.

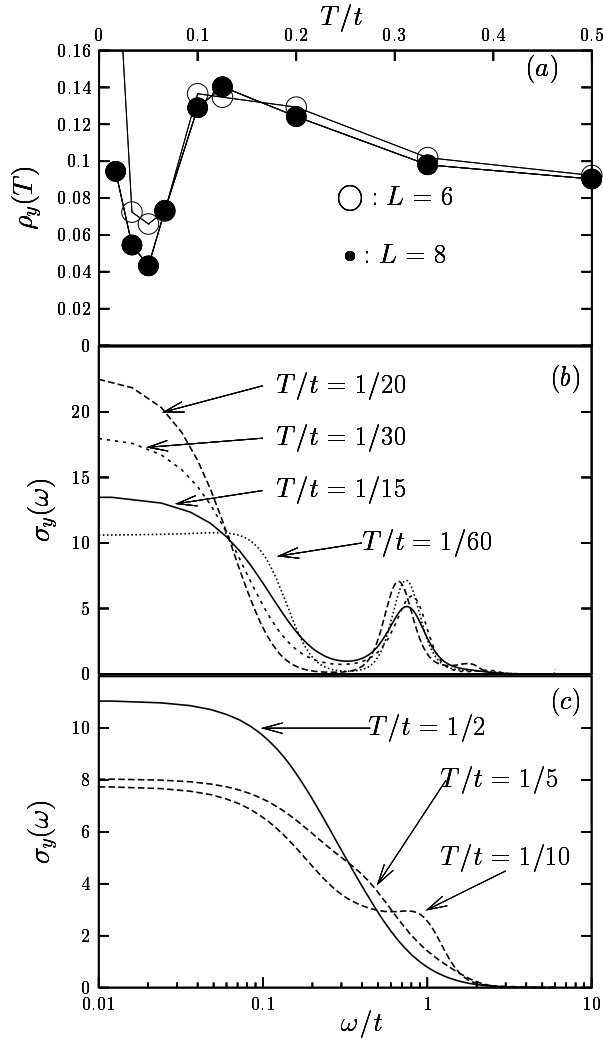


FIG. 9. Optical conductivity and related resistivity as a function of temperature at $J/t = 1.6$. The data in Figs. (b),(c) stem from simulations on lattices with 8×8 unit cells ($L=8$). In Fig. (a) both $L = 6$ and $L = 8$ results are included. As apparent and due to the inclusion of the magnetic field (see section III B) size effects are next to absent until the magnetic length scale exceeds the lattice size (see text).

Our results for the real part of the optical conductivity and associated resistivity $\rho(T) = 1/\sigma(\omega = 0, T)$ are plotted in Fig. 9. Here we consider $J/t = 1.6$. At high temperatures, $T/t = 1/2$, the data consists of a single Drude feature. As the temperature is lowered to $T/t \sim 1/10$, the weight under the Drude peak is reduced, and a feature at $\omega/t \sim 1$ is formed. A rise in the associated resistivity as a function of decreasing temperature is observed in this temperature range. This rise in resistivity originates from singular spin flip scattering on impurity spins and is reminiscent of the single impurity physics. By further reducing the temperature to $T/t \sim 1/20$ the Drude feature becomes sharper thus leading to a drop in the resistivity. Finally, at our lowest temperatures ($T/t = 1/30, 1/60$) there is a marked upturn in the resistivity. At those temperatures the optical weight under the Drude peak

starts to shift to frequencies $\omega/t \sim 0.1$.

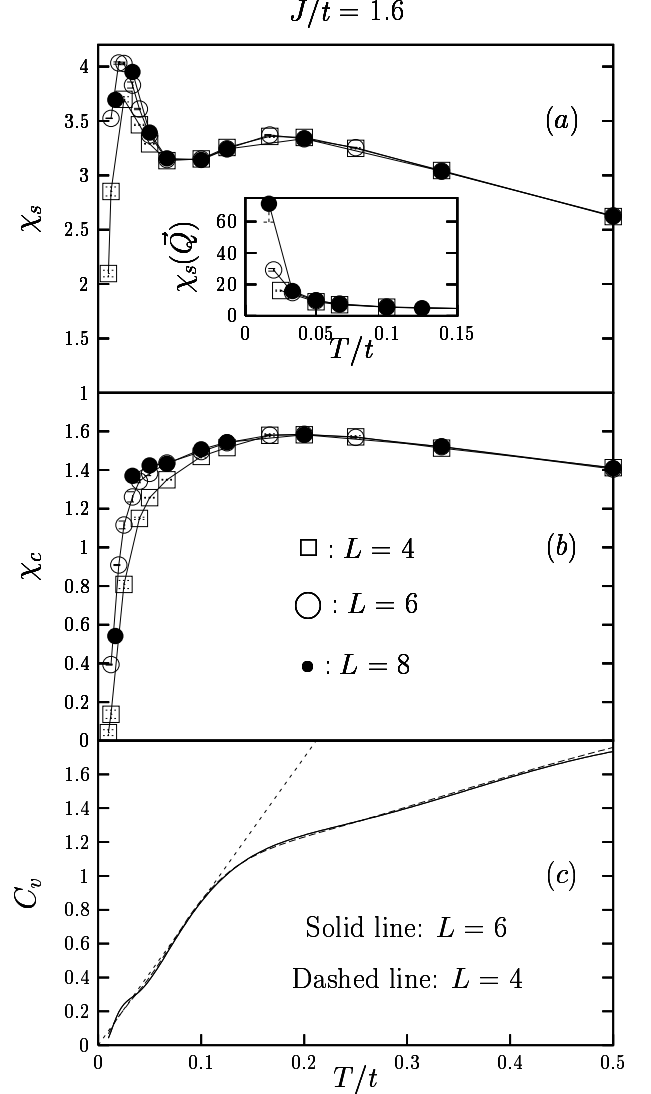


FIG. 10. (a) Uniform and staggered (inset) spin susceptibilities (b) charge susceptibilities and (c) specific heat for the DKLM at $J/t = 1.6$.

The overall form of the resistivity versus temperature curve (Fig. 9a) allows us to define three temperature scales. The highest energy scale we will discuss corresponds to the resistivity minimum, T_C . For the considered coupling $T_C \sim 0.5t$. We will define a coherence temperature $T_{coh} \sim 0.1t$ as the temperature scale at which a maximum in the resistivity is observed. The magnetic scale $T_S \sim 0.025t$ is defined by the energy scale below which the $\rho(T)$ follows an *activated* behavior. Next, we consider thermodynamic properties and concentrate on their behavior at the above defined energy scales.

Fig. 10 plots the specific heat C_v , charge and spin uniform susceptibilities (χ_c, χ_s) as well as the staggered spin susceptibility ($\chi_s(\vec{Q})$, $\vec{Q} = \vec{b}_1/2$) as a function of temperature at $J/t = 1.6$. From the technical point of

view, the specific heat is computed using the recently proposed ME based method of Ref. [18]. As apparent in the temperature region $T_S < T < T_{coh}$ one observes the following features. i) As indicated in Fig. 10c the specific heat is consistent with a γT law. ii) the uniform spin and charge susceptibilities after going through a broad maximum seem to saturate. Both points are the characteristics of a Fermi liquid. The staggered spin susceptibility essentially measures the magnetic length scale at the considered wave vector. The inset of Fig. 10a shows a marked increase in this quantity at the spin scale T_S . At the same energy scale, a *sharp* peak in the spin susceptibility is observed. Following the size effects, the data is consistent with a saturation of this quantity in the limit of zero temperature. At T_S the charge susceptibility 10b decreases rapidly. Upon analysis of size effects the data is consistent with the vanishing of this quantity at $T = 0$. Upon close analysis, an anomaly in the specific heat is apparent at T_S . Thus, T_S marks the onset of substantial spin fluctuations which triggers the formation of an insulating state which leads to the vanishing of the charge susceptibility and activated behavior of the resistivity below T_S .

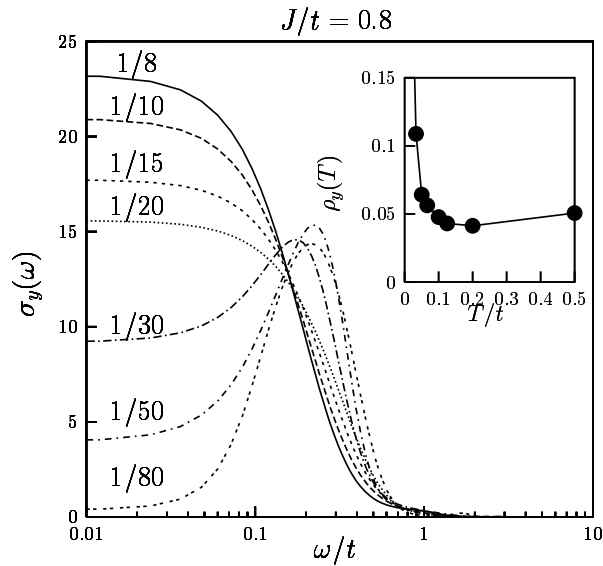


FIG. 11. Optical conductivity as a function of temperature at $J/t = 0.8$. The inset plots the resistivity versus temperature. For those simulations the lattice size is $L = 6$.

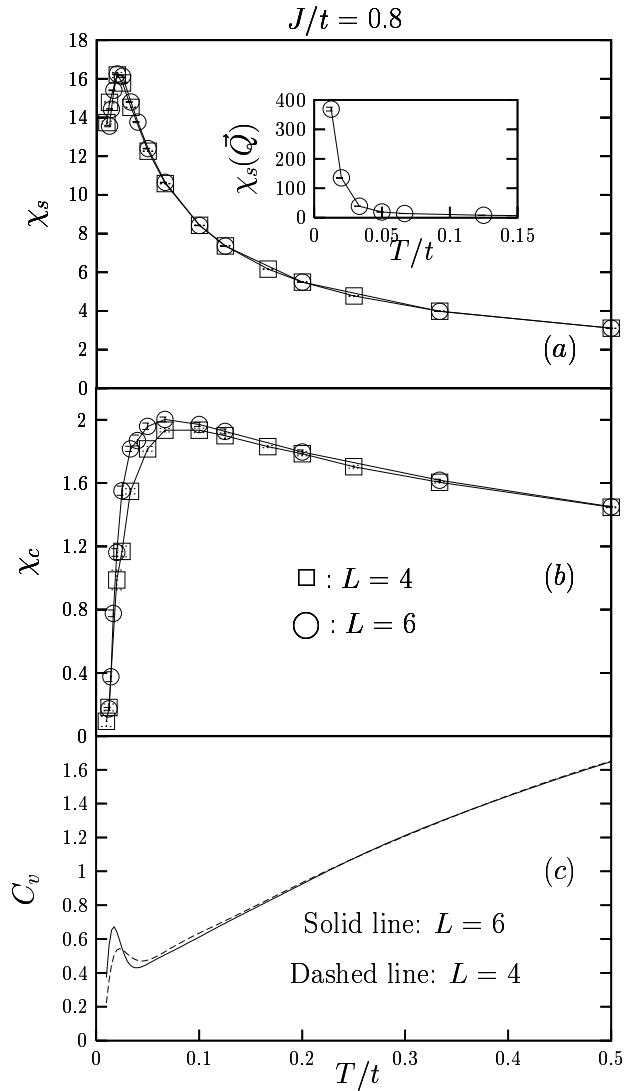


FIG. 12.

Next, we consider smaller couplings, $J/t = 0.8$. Transport and thermodynamic properties are plotted in Figs. 11 and 12. As apparent from the conductivity data (Fig. 11), no coherence scale is observed. After hitting a minimum at $T_C \sim 0.2t$ the resistivity grows monotonically as a function of decreasing temperature. The thermodynamic data of Fig. 12 equally shows no sign of the coherence scale T_{coh} . That is, there is no energy scale for which the specific heat has a linear in T dependence. The only scales which are apparent in Figs. 11 and 12 are resistivity minimum T_C and the spin scale T_S . At T_S an anomaly in C_v is detected, a drop in χ_c is observed and χ_s exhibits a sharp peak. The peak in χ_s is again located at the temperature scale at which $\chi_s(\vec{Q})$ shows a sharp increase.

Our QMC results are summarized in Fig. 13. The highest energy scale, T_C , corresponds to the resistivity minimum, triggered by enhanced spin flip scattering off the impurity spins. As already observed for the KLM, this energy scale in a first approximation tracks J . At

high temperatures, it is tempting to try to understand this energy scale in terms of the single impurity Kondo model. In this case, we can use the closed form for the impurity resistivity (see [8] and references therein):

$$R_{imp}(T) = \frac{R_0}{2} \left[1 - \frac{\ln(T/T_K)}{[\ln^2(T/T_K) + \pi^2 S(S+1)]^{1/2}} \right] \quad (20)$$

where T_K corresponds to the Kondo scale, $T_K \sim W e^{-W/J}$ and W is the bandwidth. Assuming a power-law, T^n , for the resistivity of the conduction electrons, the resistivity minimum will scale as

$$T_C \sim J^{1/n} \quad (21)$$

at weak couplings. Given the above, our QMC result $T_C \sim J$ follows by setting $n = 1$ and we are left with searching for mechanisms which will lead to a linear in T resistivity. A possibility is scattering on spin fluctuations [19–21]. Note that both the KLM [11] and DKLM an enhancement of local antiferromagnetic spin-spin correlations between impurity spin and conduction electron ($\langle \vec{S}_R^f \cdot \vec{S}_R^c \rangle$) is observed at an energy scale tracking T_C . Hence, magnetic fluctuations are potentially present at this energy scale. Clearly further work is required to justify this hand waving argument.¹

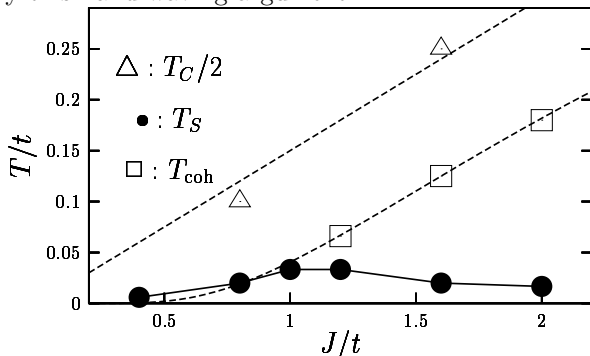


FIG. 13. Crossover scales for the DKLM as a function of J/t . T_C denotes the resistivity minimum. T_{coh} corresponds to the coherence scale at which a maximum in resistivity is observed and below which the specific heat is linear in T . Below T_S at marked increase in the magnetic length scale is observed. We use the form $e^{-1/\alpha J}$ to fit the T_{coh} and the form aT to fit the data for T_C .

Below T_C the resistivity grows as a function of decreasing temperature. For values of $J/t > 0.8$, coherence is

seen at T_{coh} . In particular, at and below T_{coh} the resistivity drops sharply, the specific shows a linear in T behavior, and both the spin and charge susceptibilities seem to converge to finite values. In a first approximation, this is what expects for a Fermi liquid. Given the limited data, it is hard to pin down the functional form of T_{coh} as a function of J/t . Nevertheless, an exponential fit ($e^{-1/\alpha J}$) accounts reasonably well for the data. Due to the particle hole symmetry of the model which automatically leads to nesting, we cannot follow the metallic state to $T = 0$. At T_S substantial spin-spin fluctuations set in and drive the system to an insulator with activated resistivity. For values of $J/t < 0.8$, the coherence temperature drops below T_S . Hence after a slow increase of resistivity below T_C , an activated behavior is expected below T_S .

Finally, we compare the QMC result to that of the mean-field calculation. In two dimensions the scales plotted in Fig. 13 are all crossover scales. As dimensionality increases, T_S will evolve to a critical temperature at which a phase transition to an ordered state occurs. On the other hand T_C and T_{coh} remain crossover scales. In the mean-field approach, both T_S and T_K mark phase transitions and the coherence temperature is a crossover scale. Comparison between the QMC (Fig. 13) and mean-field (Fig. 4) show that good agreement is obtained for T_S . Clearly, the mean-field misses completely the high energy scale T_C . The mean-field Kondo temperature compares well with the coherence temperature, T_{coh} , of the QMC data. Hence, it appears that in this specific model, when fluctuations are taken into account around the mean-field solution the mean-field Kondo scale turns out to correspond to the coherence temperature. Within our resolution, we could not pin down the much lower coherence scale predicted by the mean-field solution.

V. CONCLUSIONS

To summarize, we have presented a detailed numerical study of a depleted Kondo lattice. The depletion considered here is very special, and corresponds to the best of our knowledge to the minimal regular depletion required to obtain a two-dimensional metallic state in the $J/t \rightarrow \infty$ limit.

From the technical point of view, the QMC approach is flexible and can be applied to any depletion pattern, random or regular. The constraint to avoid the minus sign problem is the particle-hole symmetry of the conduction band. Hence various subjects may be studied. As function of depletion concentration, a metal-insulator transition should occur as observed in $\text{Ce}_3\text{Bi}_4\text{Pt}_3$ when Ce is replaced by La [4]. In the strong coupling limit one expects this metal-insulator transition to occur at the percolation threshold. Furthermore, in the insulating phase random depletion of the f -sites should trigger magnetic ordering between the magnetic moments induced by

¹Note that in comparison to the KLM [11], T_C is enhanced in the DKLM. Depleting further the DKLM of impurity spins, we should ultimately arrive to the single impurity case were T_C scales to infinity when the conduction band is modeled by free electrons.

the depletion. Hence order by disorder is equally a phenomena which can be studied in this model. To control size effects, we have introduced a magnetic field perpendicular to the two dimensional lattice. We have shown that by scaling the magnetic field as BL^2/Φ_0 extremely good size scaling to the thermodynamic limit is obtained. In particular already on small lattices the temperature scale at which size effects set in drops by an order of magnitude when the magnetic field is included. We believe that this observation will be useful for various numerical simulations of correlated electron systems.

Returning to the special choice of depletion considered here, we have compared our numerical results with a mean-field approximation. In the paramagnetic phase, this mean-field approximation reproduces the large-N saddle point [9]. Hence, we have the opportunity of comparing a widely used approximation to numerically exact results. The QMC results show three temperature scales which are summarized in Fig. 13. i) The largest scale, T_C , corresponds to the minimum in the resistivity and tracks J/t . ii) T_S corresponds to the energy scale below which the magnetic length scales grows presumably exponentially with decreasing temperature. Due to particle-hole symmetry and associated nesting properties those spin fluctuations drive the system to an insulating state. The ground state of the model remains a magnetically ordered insulator irrespective of the value of J/t . As in the KLM [11] our data supports $T_S \sim J^2$ at weak couplings, in accordance with the RKKY interaction. In the strong coupling limit T_S is exponentially suppressed and vanishes at $J/t = \infty$. Note that in the absence of nesting we expect a quantum phase transition between magnetically ordered and paramagnetic metallic states at a finite value of J/t . This is unfortunately not accessible to the QMC method due to severe sign problems. iii) The coherence temperature T_{coh} becomes apparent when it exceeds the spin scale T_S . This happens at $J/t > 0.8$. Our data is consistent with the form $T_{\text{coh}} \propto e^{-1/\alpha J}$. In the temperature range $T_{\text{coh}} < T < T_S$ we see signatures of Fermi liquid character: the specific heat is linear in T and the spin and charge susceptibilities appear to converge to finite values. Unfortunately, we cannot follow this metallic phase down to $T = 0$ because of the onset of spin fluctuations below T_S .

Comparison with the mean-field results (see Fig. 4) shows that the spin scale is well reproduced. Clearly, the T_C scale is absent in the mean-field. The mean-field Kondo temperature T_K shows a striking similarity with the QMC coherence temperature. Hence, it seems the mean-field Kondo temperature actually corresponds to a coherence scale once the model is solved exactly. Within our accuracy we have found no sign of the mean-field coherence temperature which is roughly an order of magnitude lower than the mean-field Kondo temperature.

We thank HLRS (Stuttgart) for generous allocation of CPU time on the Cray-T3E. I acknowledge useful discussions with S. Capponi, M. Feldbacher and A. Muramatsu. The Deutsche Forschungsgemeinschaft (DFG) is thanked

for financial support under the grant number AS 120/1-1.

-
- [1] P. A. Lee, T. M. Rice, J. W. Serene, L. J. Sham, and J. W. Wilkins, *Comm. Condens. Matter Phys.* **12**, 99 (1986).
 - [2] G. Aeppli and Z. Fisk, *Comm. Condens Matter Phys.* **16**, 155 (1992).
 - [3] C. Lacroix, *Solid Stat. Commun.* **54**, 991 (1985).
 - [4] M. F. Hundley, P. C. Canfield, J. D. Thompson, Z. Fisk, and J. M. Lawrence, *Phys. Rev. B* **42**, 6842 (1990).
 - [5] P. Schlottmann, *Phs. Rev. B* **54**, 12324 (1996).
 - [6] G.-M. Zhang and L. Yu, *Phys. Rev. B* **62**, 76 (2000).
 - [7] D. N. Newns and N. Read, *Adv. Phys.* **36**, 799 (1987).
 - [8] A. C. Hewson, *The Kondo Problem to Heavy Fermions, Cambridge Studies in Magnetism* (Cambridge University Press, Cambridge, 1997).
 - [9] S. Burdin, A. Georges, and D. R. Grempel, *Phys. Rev. Lett.* **85**, 1048 (2000).
 - [10] F. F. Assaad, *Phys. Rev. Lett.* **83**, 796 (1999).
 - [11] S. Capponi and F. F. Assaad, *Phs. Rev. B* **63**, (2001).
 - [12] J. R. Schrieffer and P. A. Wolff, *Phys. Rev.* **149**, 491 (1966).
 - [13] S. Doniach, *Physica B* **91**, 231 (1977).
 - [14] E. Fradkin, *Field Theories of condensed matter systems, Frontiers in Physics* (Addison-Wesley Publishing Company, Redwood City, 1991).
 - [15] D. Poilblanc, *Phys. Rev. B* **44**, 9562 (1991).
 - [16] C. Gross, *Z. Phys. B* **86**, 359 (1992).
 - [17] M. Jarrell and J. Gubernatis, *Physics Reports* **269**, 133 (1996).
 - [18] C. Huscroft, R. Gass, and M. Jarrell, *Phys. Rev. B* **61**, 9300 (2000).
 - [19] P. Monthoux and D. Pines, *Phys. Rev. B* **49**, 4261 (1994).
 - [20] T. Moriya, Y. Takahashi, and K. Ueda, *J. Phys. Soc. Jpn.* **59**, 2905 (1990).
 - [21] R. Hlubina and T. M. Rice, *Phys. Rev. B* **51**, 9253 (1995).